Deep-red double-clad fiber laser at 717 nm

Esrom Kifle, Pavel Loiko, Thibaud Berthelot, Thiphaine Rault, Laurine Bodin, Florence Pau, Gilles Recoque, Thierry Georges, Patrice Camy

Deep-red double-clad fiber laser at 717 nm

ESROM KIFLE,[1] PAVEL LOIKO,[1] THIBAUD BERTHELOT,[2] THIPHAINE RAULT,[2] LAURINE BODIN,[2] FLORENCE PAU,[3] GILLES RECOQUE,[3] THIERRY GEORGES,[3] AND PATRICE CAMY[1,*]

[1]Centre de Recherche sur les Ions, les Matériaux et la Photonique (CIMAP), UMR 6252 CEA-CNRS-ENSICAEN, Université de Caen Normandie, 6 Boulevard Maréchal Juin, 14050 Caen Cedex 4, France
[2]Le Verre Fluoré, rue Gabriel Voisin, Campus de Ker-Lann, 35170 Bruz, France
[3]Oxxius SA, 4 rue Louis de Broglie 22300 Lannion
**Corresponding author: patrice.camy@ensicaen.fr*

Received XX Month XXXX; revised XX Month, XXXX; accepted XX Month XXXX; posted XX Month XXXX (Doc. ID XXXXX); published XX Month XXXX

We report on a double-clad fiber laser operating on the $^3P_0 \rightarrow {}^3F_4$ Pr^{3+} transition (in the deep-red spectral range) pumped by a GaN diode laser at ~442 nm. It employed a 0.8 mol% PrF_3-doped ZBLAN double-clad fiber with a 7.5 µm core, a double D-shaped inner cladding, and a length of 3.0 m. The laser delivered a maximum output power of 0.71 W at 716.7 nm with a slope efficiency of 9.0 % (vs. the launched pump power) and a laser threshold of 0.90 W. The laser emission was partially polarized. The laser performance was simulated providing a guideline for watt-level deep-red fiber laser sources. © 2022 Optical Society of America

http://dx.doi.org/10.1364/OL.99.099999

Deep-red (far-red) light is the emission at the red end of the visible spectrum, between 660 and 750 nm. It is hardly visible by a naked eye, but it plays a key role in many biological processes such as photosynthesis due to intense absorption of chlorophyll at these wavelengths. Deep-red lasers find applications in bio-photonics, live cell imaging experiments [1] and studying the dynamics of free radicals in DNA chains [2], bio-medicine [3] and UV generation by frequency doubling with potential application in food safety [4,5]. Deep-red emission can be directly generated using several rare-earth ions such as Pr^{3+} [6], Eu^{3+} [7], and Ho^{3+} [8], as shown in Fig. 1. Among them, praseodymium (Pr^{3+}) ions (electronic configuration: $[Xe]4f^2$) are the most attractive ones owing to the possibility of their efficient pumping by commercial and powerful blue GaN diodes emitting at ~442 nm [9,10]. The deep-red Pr^{3+} emission at ~717 nm originates from the $^3P_0 \rightarrow {}^3F_4$ transition.

There exist multiple studies on deep-red solid-state lasers based on Pr^{3+}-doped crystals [11-13]. Fiber lasers, in their turn, benefit from a small footprint, high output beam quality, flexible design and good thermal management. So far, there are only a few reports on Pr^{3+}-based fiber laser sources operating in the deep-red spectral range mainly because of the difficulty of suppressing oscillations on the competitive high-gain red laser transition. All of them employed fluoride fibers (the ZBLAN glass system) to benefit from attractive spectroscopic properties of Pr^{3+} ions in these materials, i.e., low phonon energies (~580 cm^{-1}) leading to weak non-radiative path and long luminescence lifetimes of the $^3P_0$ state [14], and relatively high position (~50000 cm^{-1}) of energy-levels of the excited $4f^15d^1$ configuration avoiding the detrimental excited-state absorption to these levels [15]. Like other glasses, Pr^{3+}:ZBLAN ones also benefit from broad absorption and emission spectra facilitating diode-pumping and allowing for wavelength tunable operation.

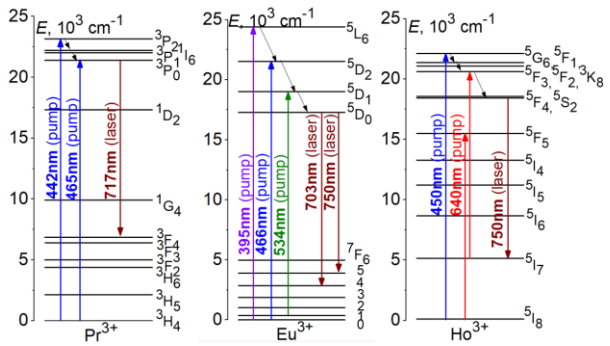

Fig. 1. Energy-level schemes of Pr^{3+}, Eu^{3+} and Ho^{3+} ions showing pump and deep-red laser transitions.

First continuous-wave (CW) and tunable operation of a deep-red Pr:ZBLAN fiber laser was reported by Allain *et at.* using a 0.12 mol% Pr^{3+}-doped, 12 µm core diameter, 60 cm long fiber. Under pumping by an Ar^+ ion laser at 476.5 nm, the Pr fiber laser delivered 50 mW at 715 nm with a threshold of 230 mW and a tuning range of 707-725 nm [6]. Later, a similar laser was exploited by Smart *et al.* leading to a high laser slope efficiency of 30% (vs. the launched pump power) and a laser threshold of only 40 mW [16]. Using a GaN laser diode to pump a 0.3 mol% Pr^{3+}-doped, 3.9 µm core diameter, 9 cm long ZBLAN fiber, Okamoto *et al.* achieved 49 mW at 716 nm with slope efficiency of 30% and a threshold of 21 mW, and

demonstrated an ultrabroadband tuning range of 597-737 nm [17]. Li *et al.* reported on passive Q-switching of a similar all-fiber laser using single-walled carbon nanotubes leading to a pulse duration / energy of 2.3 μs / 18.3 nJ at a repetition rate of 86.5 kHz [18].

All the above-described lasers were based on single-clad fibers with core pumping and so far, there are no reports on double-clad deep-red fiber lasers. The double-clad fiber geometry is beneficial for high-power diode-pumping due to the large numerical aperture of the inner cladding allowing for efficient pump coupling and a distributed absorption over the fiber length and better thermal management. Recently, watt-level diode-pumped red (~635 nm) double-clad Pr fiber lasers were demonstrated [10,19,20]. In the present work, we aimed to develop a high-power deep-red double-clad Pr fiber laser with an open-space GaN diode pumping.

At first, we revisited the spectroscopic properties of Pr^{3+} ions in a 0.8 mol% PrF_3-doped ZBLAN glass relevant for the deep-red laser operation. The absorption cross-sections, σ_{abs}, in the blue spectral range (the $^3H_4 \rightarrow {}^3P_2$ transition) are shown in Fig. 2(a). The peak σ_{abs} is 1.08×10^{-20} cm^2 at 442 nm and the absorption bandwidth (FWHM) is 9.5 nm. This band well overlaps with the emission of blue GaN laser diodes (LD). Figure 2(a) depicts an example drift of the central wavelength of a GaN LD from 436.3 to 444.9 nm with increasing the forward driving current from 0.5 to 8 A.

The stimulated-emission (SE) cross-sections, σ_{SE}, for the $^3P_0 \rightarrow {}^3F_4$ transition falling into the deep-red spectral range were calculated using the Füchtbauer–Ladenburg equation to be 2.03×10^{-20} cm^2 at 716.5 nm. Here, we considered a radiative lifetime $\tau_{rad}(^3P_0)$ of 42 μs and a luminescence branching ratio $\beta(JJ')$ of 14.3% [14]. For comparison, for the $^3P_0 \rightarrow {}^3F_2$ transition in the red, the peak σ_{SE} is 4.22×10^{-20} cm^2 at 635.3 nm, Fig.2(b). It is expected to be a source of a strong gain competition for a deep-red laser. For 0.8 mol% PrF_3 doping, the luminescence lifetime of the $^3P_0$ state is 37.5 μs.

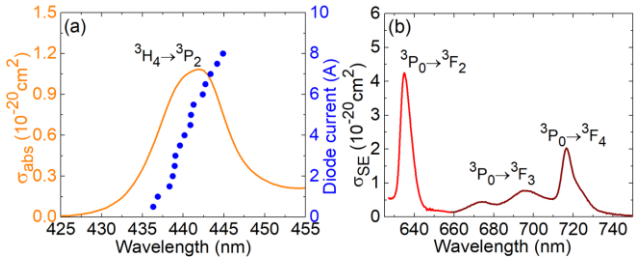

Fig. 2. Spectroscopy of Pr^{3+} ions in the ZNLAN glass: (a) absorption cross-sections, σ_{abs}, for the $^3H_4 \rightarrow {}^3P_2$ transition, *circles* – shift of the emission wavelength of a GaN diode laser *vs.* the driving current; (b) stimulated-emission (SE) cross-sections, σ_{SE}, for the red ($^3P_0 \rightarrow {}^3F_2$) and deep-red ($^3P_0 \rightarrow {}^3F_{3,4}$) transitions.

A Pr^{3+}-doped ZBLAN fluoride fiber (Le Verre Fluoré) with a double-clad geometry was used as a gain medium. The core had a doping level of 0.8 mol% PrF_3 ($N_{Pr} = 1.55\times10^{20}$ cm^{-3}) and a diameter of 7.5 μm. The inner cladding was made of a lower-index fluoride glass having a truncated circular (double D-shaped) profile (diameters: 115/125 μm) to enhance the pump absorption in the core. The outer cladding was made of a resin polymer having a diameter of 180 μm. The numerical aperture (N.A.) of the fiber was 0.45 (inner cladding, guiding the pump) and 0.08 (core, propagating the laser radiation). The fiber core supported up to 2 modes at the deep-red laser wavelength (LP_{01} and LP_{11}, calculated confinement factors: 87.8% and 57.0%, respectively). In the red, it also supported 2 modes with 90.6% (LP_{01}) and 69.2% (LP_{11}) confinement factors. The cut-off wavelength of the fiber was 0.78 μm. The mode field diameter was 7.54 μm (core, LP_{01} mode, deep-red emission).

The pump absorption in the fiber at a low incident pump power P_{inc} of 1.0 W was determined from pump-transmission (cut-back) measurements for several fiber lengths L, Fig. 3(a). With increasing L from 0.4 to 4.5 m, the pump attenuation gradually increased from 39.5% to 96.0% (including both the pump absorption, α_{abs}, and the propagation losses in the cladding, $\alpha_{loss,clad}$). The points in Fig. 3(a) were fitted using the formula $1 - \exp(-(\alpha_{abs}\times\Gamma_p + \alpha_{loss,clad})L)$, where $\alpha_{abs} = 0.48\times10^3$ dB/m (small-signal value, from the spectroscopic data), $\alpha_{loss,clad} = 1.17 \pm 0.2$ dB/m (estimated from cut-back measurements) and $\Gamma_p = 3.6\times10^{-3}$ is the power filling factor (taken as the ratio of the core / clad fiber areas). Figure 3(b) summarizes the propagation losses in the core / inner cladding. For the core, $\alpha_{loss,core}$ is as low as 0.23±0.1 dB/m at 633 nm. For the inner cladding, the observed loss values are explained by the parasitic absorption of blue light in the UV-curable resin polymer. The dependence of pump transmission through a 5 m-long fiber on the incident pump power is shown in Fig. 3(c). It is due to the temperature drift of the diode wavelength.

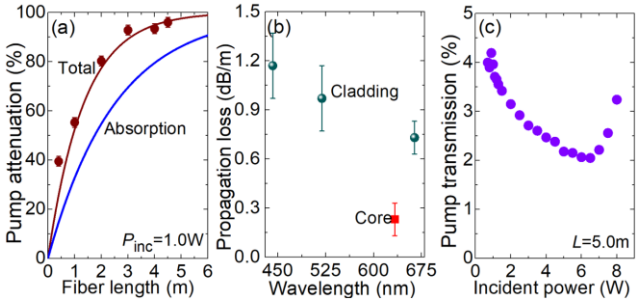

Fig. 3. Characterization of the double-clad Pr^{3+}-doped fluoride fiber: attenuation of the pump radiation from a GaN diode *vs.* the fiber length at P_{inc} = 1.0 W: *symbols* – experimental data, *curves* – simulation: pump absorption and losses (*solid curve*), pump absorption only (*dashed curve*); (b) propagation losses for the fiber inner cladding and core; (c) pump transmission vs. the incident pump power for a 5.0 m-long fiber.

The scheme of the laser is depicted in Fig. 4 (the fiber design is shown at the inset). As a pump source, we used an open-space GaN laser diode (NUBM44, Nichia) with a super-Gaussian output beam profile. The pump radiation was collimated using an antireflection (AR) coated cylindrical short focal length (f = 1.19 mm) lens (LIMO) and focused into the fiber using an AR-coated aspherical lens (f = 6 mm, Thorlabs). The mode diameter (at the $1/e^2$ level) at the fiber input facet was measured to be 80×60±5 μm^2 well fitting the inner cladding size. We estimated the pump coupling efficiency from the Fresnel loss at the uncoated fiber facet to be ~96%. A dichroic folding mirror coated for high transmission (HT, $T > 98\%$) at 325 - 500 nm and high reflection (HR, $R > 99.8\%$) at 525 – 800 nm was inserted before the focusing lens at an angle of 45°. GaN LDs could be operated beyond the nominal output power in the so-called overdrive pulse mode [21]. We have used a single-emitter GaN LD with a nominal output of 4.7 W at a forward current of 4 A. In the overdrive pulse mode, its peak power was scaled up to 10 W at a repetition rate of 67 Hz and a duty cycle of 10% (pulse duration: 1.5 ms, quasi-CW pumping). The LD was mounted on a copper heat-sink and kept at 17 °C using circulating water.

A fiber with a length of 3.0 m was used for the laser experiment. The pump attenuation was 92.8±2% (pump absorption: ~69.5%), Fig. 2(a). The input facet of the fiber was flat-cleaved and the output one was polished at an angle of 8° to suppress the unwanted Fresnel reflection causing lasing in the red. Both fiber ends were placed on V-groove holders for passive cooling. An intracavity AR-coated (350 - 700 nm) aspherical lens (f = 11 mm) was used to collimate the emission from the polished output fiber end. An intracavity AR-coated SF10 prism placed at the Brewster's angle was additionally implemented to disperse the red / deep-red emissions. The cavity was formed by a flat rear mirror M1 (R > 99.7% at 717 nm), a flat dichroic folding mirror DM and a flat output coupler M2 (T_{OC} = 41.7% at 717 nm). To suppress the unwanted lasing at the high gain $^3P_0 \rightarrow {}^3F_2$ Pr^{3+} transition in the red, both the M1 and M2 mirrors were coated for high transmission at 635 nm (T = 47.0% and 82.3%, respectively). It was critical to use both the intracavity prism for the spatial beam separation and spectrally selective mirrors to obtain deep-red laser emission (without the prism, only red laser line was generated). To compare with the red laser transition, another pair of M1' (HR at 635 nm) and M2' (T_{OC} = 95% at 635 nm) mirrors was used. A long-pass filter (FEL550, Thorlabs) was used to filter out the residual pump. The laser spectra were measured using an optical spectrum analyzer (Ando AQ-6315E, SBW = 0.05 nm).

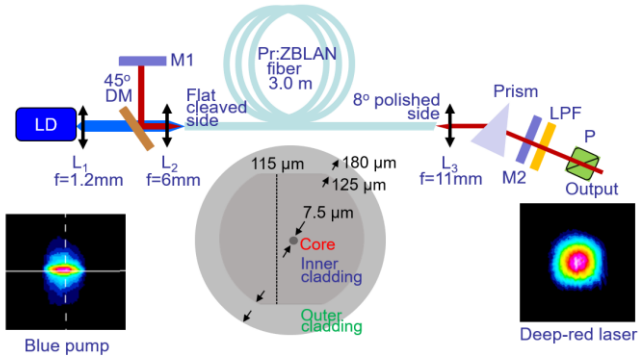

Fig. 4. Scheme of the diode-pumped double-clad deep-red fiber laser: M1 – rear mirror, M2 – output coupler, LD – laser diode, $L_{1\text{-}3}$ – lenses, DM – dichroic mirror (45°), LPF – long-pass filter, P – polarizer, *inset* - cross-section of the double-clad fiber. *Insets* – beam profiles of the pump (at the input fiber facet) and laser radiation (in the far-field).

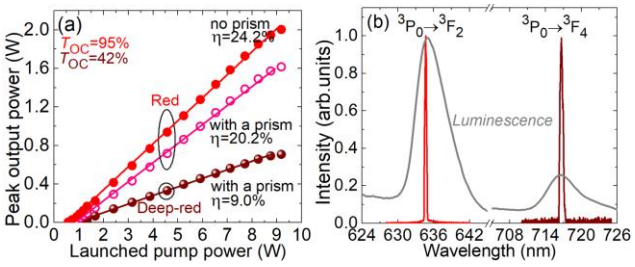

Fig. 5. Diode-pumped deep-red / red Pr fiber lasers: (a) input-output dependences, η – slope efficiency; (b) typical spectra of laser emission, *grey curve* – luminescence spectrum.

The input-output dependence of the Pr^{3+} double-clad fiber laser operating on the $^3P_0 \rightarrow {}^3F_4$ transition is shown in Fig. 5(a). For the studied M2 mirror with T_{OC} = 41.7%, the deep-red laser generated a maximum peak output power of 0.71 W at 716.7 nm with a slope efficiency η of 9.0% / 13.0% (*vs.* the launched / absorbed pump power, respectively) and a laser threshold of 0.90 W, representing the highest output power for this type of lasers. The laser linewidth (FWHM) was 0.6 nm, Fig. 5(b). The deep-red Pr fiber laser operated on the fundamental transverse mode (LP_{01}) with a measured beam quality factor M^2 < 1.1 at the maximum output level. No colasing at the red wavelength was observed.

When using the M1' and M2' mirrors and removing the prism from the cavity, the laser operated on the $^3P_0 \rightarrow {}^3F_2$ transition (in the red) delivering a maximum peak output power of 2.0 W at 634.5 nm with η of 24.2% / 34.8% (*vs.* the launched / absorbed pump power) and a reduced laser threshold of 0.57 W. A slight roll-over in the output dependences for launched pump powers above 9 W for both lasers is due to the temperature-induced shift of the LD wavelength resulting in a reduction of the pump absorption efficiency in the fiber, cf. Fig. 2(a). The laser linewidth was 0.4 nm.

The polarization state of the laser was studied using a polarizing prism. For both studied laser transitions, the emission was partially polarized. The polarization degree, $P = (P_{max} - P_{min})/(P_{max} + P_{min})$, was pump-dependent, Fig. 6(a). For the deep-red laser, it was high near the threshold (P = 0.67), exhibited a minimum at an intermediate power and increased again reaching P = 0.49 at P_{launch} = 9.2 W. This corresponded to 0.53 W of linearly polarized deep-red emission. The corresponding polar plot of the polarization-dependent output power is shown in Fig. 6(b). The polarization direction was along the horizontal axis (being close to the larger diameter of the inner cladding). A similar but less pronounced dependence was observed for the red laser. Such a behavior was not described previously for double-clad Pr:ZBLAN fiber lasers. The observed polarization behavior is assigned to the intrinsic anisotropy (birefringence) of the double D-shaped double-clad fiber. The observed pump dependence of P is probably induced by the thermal distortion of the fiber upon high-power diode pumping. We believe that higher P values for the deep-red fiber laser are due to the stronger heat loading for the $^3P_0 \rightarrow {}^3F_4$ transition causing thermal distortion.

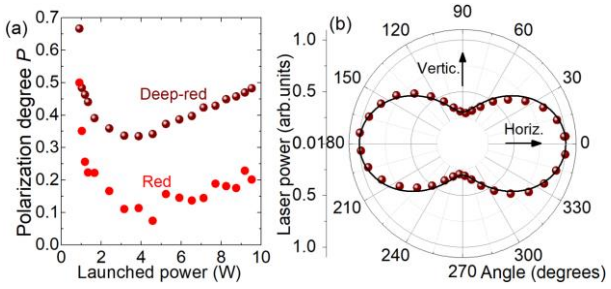

Fig. 6. Polarization effects in the deep-red / red double-clad Pr fiber lasers: (a) polarization degree (P) of laser emission; (b) normalized polar plot of the polarization-dependent output power for the deep-red laser, launched pump power: P_{launch} = 9.2 W.

The performance of the deep-red Pr fiber laser was simulated using the model of a strongly pumped quasi-four-level laser [22]. The double-clad fiber design depicted in Fig. 4 was considered. The spectroscopic parameters of Pr^{3+} ions in the ZBLAN glass and the loss characteristics of the fiber described above were used. An extra passive loss of 2.7 dB (single-pass) was considered accounting for

the intracavity elements (lenses, prism) and imperfections of the cleaved and polished fiber facets. The results are shown in Fig. 7. The calculated input-output dependence reasonably well fits with the experimental one, Fig. 7(a). There exists an optimum fiber length of ~1.5 m which is determined by a counterplay between increasing pump absorption and raising cavity roundtrip losses, see Fig. 7(b). For lower losses in the fiber / cavity, it is expected that the optimum L value will increase. For a fixed launched pump power, the deep-red output is expected to increase monotonically with the output coupling, Fig. 7(c). This dependence is due to the relatively low level of passive losses in the fiber core and it agrees with the experimental data for red Pr:ZBLAN double-clad fiber lasers [10]. For higher losses in the fiber (passive loss / reabsorption for a quasi-three-level laser scheme, e.g., cyan lasers), a local maximum in such a dependence will be observed. For T_{OC} > 50%, a watt-level deep-red output is expected. Note that such a mirror would still need to ensure HT at 635 nm to suppress the competitive high-gain red laser transition (it was not available in our experiment).

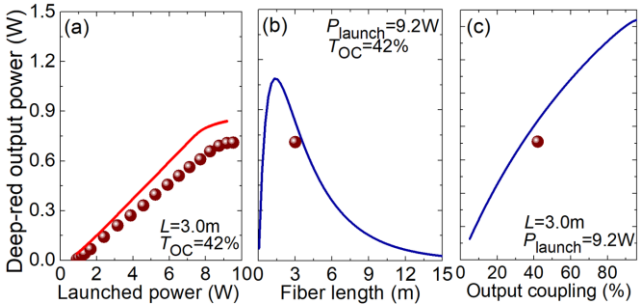

Fig. 7. Simulated output power of a deep-red Pr fiber laser: (a) vs. the launched pump power, L = 3.0 m, T_{OC} = 42%,; (b) vs. the fiber length, T_{OC} = 42%, P_{launch}= 9.2 W; (c) vs. the output coupling, L = 3.0 m, P_{launch}= 9.2 W, *circles* – experiment, *curves* – simulation. Other simulation parameters are listed in the text.

To conclude, we report on a deep-red (717 nm) fiber laser based on a Pr^{3+}-doped double-clad fluoride fiber with a double D-shaped inner cladding allowing for efficient GaN laser diode pumping. The power scaling of the fiber laser was attained by operating the diode in the overdrive pulse mode (quasi-CW pumping). The suppression of the competitive high gain red laser transition was ensured by using an intracavity prism for the spatial beam separation. The deep-red laser emission was partially polarized; the polarization degree was pump-dependent increasing with the pump power well above the laser threshold. This is assigned to the intrinsic optical anisotropy of the double D-shaped double-clad fiber and its thermal distortion under high-power diode pumping. In our experiment, the Pr:ZBLAN double-clad fiber laser delivered 0.71 W at 716.7 nm with a slope efficiency of 9.0% (*vs.* the pump power launched into the fiber), representing the highest output power for this type of lasers. The output performance of deep-red double-clad diode-pumped Pr fiber lasers was simulated yielding a route for further power scaling, i.e., by using an optimum fiber length of ~1.5 m (this value depends on the actual level of losses in the fiber) and high output coupling (T_{OC} > 90%). In this way, watt-level output is expected, so that deep-red double-clad Pr:ZBLAN fiber lasers could outperform bulk Eu [7] and Pr [11] laser sources. Further efforts are needed to improve the polarization degree of the deep-red laser emission.

Funding. French Government (the Future Investments Program), and Bretagne and Normandy regions (FIZIC project).

Disclosures. The authors declare no conflicts of interest.

Data Availability. Data underlying the results presented in this paper are not publicly available at this time but may be obtained from the authors upon reasonable request.

References

1. A. Diaspro, D. Silvano, S. Krol, O. Cavalleri, and A. Gliozzi, Langmuir **18**, 5047 (2002).
2. E. Balanikas, A. Banyasz, G. Baldacchino, and D. Markovitsi, Molecules **24**, 2347 (2019).
3. P. Agostinis, K. Berg, K. A. Cengel, T. H. Foster, A. W. Girotti, S. O. Gollnick, S. M. Hahn, M. R. Hamblin, A. Juzeniene, D. Kessel, M. Korbelik, J. Moan, P. Mroz, D. Nowis, J. Piette, B. C. Wilson, and J. Golab, CA: Cancer J. Clin. **61**, 250 (2011).
4. Q. Wu and H. Xu, Food Chem. **290**, 24 (2019).
5. V. Ostroumov, W. Seelert, L. Hunziker, C. Ihli, A. Richter, E. Heumann, and G. Huber, Proc. SPIE **6451**, 645103 (2007).
6. J. Allain, M. Monerie, and H. Poignant, Electronics Letters **27**(2), 189 (1991).
7. P. Loiko, D. Rytz, S. Schwung, P. Pues, T. Jüstel, J.-L. Doualan, and P. Camy, Opt. Lett. **46**, 2702 (2021).
8. S. Ji, S. Huang, Z. Wang, X. Lin, B. Xiao, H. Xu, and Z. Cai, J. Lightwave Technol., doi: 10.1109/JLT.2022.3211182 (2022).
9. J. Nakanishi, Y. Horiuchi, T. Yamada, O. Ishii, M. Yamazaki, M. Yoshida, and Y. Fujimoto, Opt. Lett. **36**, 1836 (2011).
10. E. Kifle, F. Starecki, P. Loiko, S. Cozic, F. Joulain, T. Berthelot, T. Georges, D. Stojcevski, D. Deubel, and P. Camy, Opt. Lett. **46**, 74 (2021).
11. M. He, S. Chen, Q. Na, S. Luo, H. Zhu, Y. Li, C. Xu, and D. Fan, Chin. Opt. Lett. **18**, 011405 (2020).
12. X. Lin, X. Huang, B. Liu, B. Xu, H. Xu, Z. Cai, X. Xu, D. Li, J. Liu, and J. Xu, Opt. Mater. **76**, 16 (2018).
13. S. Luo, X. Yan, Q. Cui, B. Xu, H. Xu, and Z. Cai, Opt. Commun. **380**, 357 (2016).
14. M. Olivier, J.-L. Doualan, V. Nazabal, P. Camy, and J.-L. Adam, J. Opt. Soc. Am. B **30**, 2032 (2013).
15. C. Kränkel, D. T. Marzahl, F. Moglia, G. Huber, and P. W. Metz, Laser Photon. Rev. **10**, 548 (2016).
16. R. G. Smart, J. N. Carter, A. C. Tropper, D. C. Hanna, S. T. Davey, S. F. Carter, and D. Szebesta, Opt. Commun. **86**, 333 (1991).
17. H. Okamoto, K. Kasuga, I. Hara, and Y. Kubota, Opt. Express **17**, 20227 (2009).
18. W. Li, T. Du, J. Lan, C. Guo, Y. Cheng, H. Xu, C. Zhu, F. Wang, Z. Luo, and Z. Cai, "716 nm deep-red passively Q-switched Pr:ZBLAN all-fiber laser using a carbon-nanotube saturable absorber," Opt. Lett. **42**, 671 (2017).
19. M.-P. Lord, V. Fortin, F. Maes, L. Talbot, M. Bernier, and R. Vallée, Opt. Lett. **46**, 2392 (2021).
20. S. Liu, J. Lin, S. Ji, Y. Song, Q. Feng, B. Xiao, Z. Wang, H. Xu, and Z. Cai, Opt. Laser Technol. **157**, 108720 (2023).
21. Y. Fujitomo, M. Murakami, J. Nakanishi, T. Yamada, O. Ishii, and M. Yamazaki, in *Advanced Solid-State Lasers Congress*, OSA Technical Digest (Optica Publishing Group, 2013), P. AM2A.2.
22. I. Kelson and A. A. Hardy, IEEE J. Quantum Electron. **34**, 1570 (1998).

Full references

1. A. Diaspro, D. Silvano, S. Krol, O. Cavalleri, and A. Gliozzi, "Single living cell encapsulation in nano-organized polyelectrolyte shells," Langmuir **18**(13), 5047-5050 (2002).
2. E. Balanikas, A. Banyasz, G. Baldacchino, and D. Markovitsi, "Populations and dynamics of guanine radicals in DNA strands—direct versus indirect generation," Molecules **24**(13), 2347 (2019).
3. P. Agostinis, K. Berg, K. A. Cengel, T. H. Foster, A. W. Girotti, S. O. Gollnick, S. M. Hahn, M. R. Hamblin, A. Juzeniene, D. Kessel, M. Korbelik, J. Moan, P. Mroz, D. Nowis, J. Piette, B. C. Wilson, and J. Golab, "Photodynamic therapy of cancer: an update," CA: Cancer J. Clin. **61**, 250-281 (2011).
4. Q. Wu and H. Xu, "Application of multiplexing fiber optic laser induced fluorescence spectroscopy for detection of aflatoxin B1 contaminated pistachio kernels," Food Chem. **290**, 24-31 (2019).
5. V. Ostroumov, W. Seelert, L. Hunziker, C. Ihli, A. Richter, E. Heumann, and G. Huber, " UV generation by intracavity frequency doubling of an OPS-pumped Pr:YLF laser with 500 mW of cw power at 360 nm," Proc. SPIE **6451**, 645103 (2007).
6. J. Allain, M. Monerie, and H. Poignant, "Tunable CW lasing around 610, 635, 695, 715, 885 and 910 nm in praseodymium-doped fluorozirconate fibre," Electronics Letters **27**(2), 189-191 (1991).
7. P. Loiko, D. Rytz, S. Schwung, P. Pues, T. Jüstel, J.-L. Doualan, and P. Camy, "Watt-level europium laser at 703 nm," Opt. Lett. **46**(11), 2702-2705 (2021).
8. S. Ji, S. Huang, Z. Wang, X. Lin, B. Xiao, H. Xu, and Z. Cai, "Watt-level high-efficiency deep-red Ho^{3+}:ZBLAN fiber laser," J. Lightwave Technol., doi: 10.1109/JLT.2022.3211182 (2022).
9. J. Nakanishi, Y. Horiuchi, T. Yamada, O. Ishii, M. Yamazaki, M. Yoshida, and Y. Fujimoto, "High-power direct green laser oscillation of 598 mW in Pr^{3+}-doped waterproof fluoroaluminate glass fiber excited by two-polarization-combined GaN laser diodes," Opt. Lett. **36**(10), 1836-1838 (2011).
10. E. Kifle, F. Starecki, P. Loiko, S. Cozic, F. Joulain, T. Berthelot, T. Georges, D. Stojcevski, D. Deubel, and P. Camy, "Watt-level visible laser in double-clad Pr^{3+}-doped fluoride fiber pumped by a GaN diode," Opt. Lett. **46**(1), 74-77 (2021).
11. M. He, S. Chen, Q. Na, S. Luo, H. Zhu, Y. Li, C. Xu, and D. Fan, "Watt-level Pr^{3+}:YLF deep red laser pumped by a fiber-coupled blue LD module or a single-emitter blue LD," Chin. Opt. Lett. **18**(11), 011405-1-5 (2020).
12. X. Lin, X. Huang, B. Liu, B. Xu, H. Xu, Z. Cai, X. Xu, D. Li, J. Liu, and J. Xu, "Continuous-wave laser operation at 743 and 753 nm based on a diode-pumped c-cut Pr:$YAlO_3$ crystal," Opt. Mater. **76**, 16-20 (2018).
13. S. Luo, X. Yan, Q. Cui, B. Xu, H. Xu, and Z. Cai, "Power scaling of blue-diode-pumped Pr:YLF lasers at 523.0, 604.1, 606.9, 639.4, 697.8 and 720.9nm," Opt. Commun. **380**, 357-360 (2016).
14. M. Olivier, J.-L. Doualan, V. Nazabal, P. Camy, and J.-L. Adam, "Spectroscopic study and Judd–Ofelt analysis of Pr^{3+}-doped Zr–Ba–La–Al glasses in visible spectral range," J. Opt. Soc. Am. B **30**(8), 2032-2042 (2013).
15. C. Kränkel, D. T. Marzahl, F. Moglia, G. Huber, and P. W. Metz, "Out of the blue: semiconductor laser pumped visible rare-earth doped lasers," Laser Photon. Rev. **10**(4), 548-568 (2016).
16. R. G. Smart, J. N. Carter, A. C. Tropper, D. C. Hanna, S. T. Davey, S. F. Carter, and D. Szebesta, "CW room temperature operation of praseodymium-doped fluorozirconate glass fibre lasers in the blue-green, green and red spectral regions," Opt. Commun. **86**(3), 333-340 (1991).
17. H. Okamoto, K. Kasuga, I. Hara, and Y. Kubota, "Visible–NIR tunable Pr^{3+}-doped fiber laser pumped by a GaN laser diode," Opt. Express **17**(22), 20227-20232 (2009).
18. W. Li, T. Du, J. Lan, C. Guo, Y. Cheng, H. Xu, C. Zhu, F. Wang, Z. Luo, and Z. Cai, "716 nm deep-red passively Q-switched Pr:ZBLAN all-fiber laser using a carbon-nanotube saturable absorber," Opt. Lett. **42**(4), 671-674 (2017).
19. M.-P. Lord, V. Fortin, F. Maes, L. Talbot, M. Bernier, and R. Vallée, "2.3 W monolithic fiber laser operating in the visible," Opt. Lett. **46**(10), 2392-2395 (2021).
20. S. Liu, J. Lin, S. Ji, Y. Song, Q. Feng, B. Xiao, Z. Wang, H. Xu, and Z. Cai, "High-power tunable red laser based on double-cladding Pr^{3+}-doped fiber," Opt. Laser Technol. **157**, 108720 (2023).
21. Y. Fujitomo, M. Murakami, J. Nakanishi, T. Yamada, O. Ishii, and M. Yamazaki, "Visible lasers in waterproof fluoro-aluminate glass fibers excited by GaN laser diodes," in *Advanced Solid-State Lasers Congress*, OSA Technical Digest (Optica Publishing Group, 2013), P. AM2A.2.
22. I. Kelson and A. A. Hardy, "Strongly pumped fiber lasers," IEEE J. Quantum Electron. **34**(9), 1570-1577 (1998).